RSC Advances

PAPER

View Article Online
View Journal | View Issue

Cite this: *RSC Adv.*, 2024, **14**, 25908

Molecular insight into binding affinities and blockade effects of selected flavonoid compounds on the PD-1/PD-L1 pathway†

Yan Guo, [a] Jinchang Tong,[a] Jianhuai Liang,[b] Kaixin Shi,[a] Xinyue Song,[a] Zichao Guo,[a] Boping Liu*[b] and Jianguo Xu *[a]

This study investigated the binding mechanisms of the flavonoids apigenin (Api), kaempferol (Kmp), and quercetin (Que) to the PD-L1 dimer using a combination of molecular modeling and experimental techniques. The binding free energy results demonstrated that the flavonoids could tightly bind to the PD-L1 dimer, with the binding abilities following the trend Que > Kmp > Api. Key residues Ile54, Tyr56, Met115, Ala121, and Tyr123 were identified as important for binding. The flavonoids primarily bind to the C-, F-, and G-sheet domains. The spontaneous formation of the complex systems was mainly driven by hydrophobic forces. Dynamic cross-correlation matrix and secondary structure analyses further indicated that the studied flavonoids could stably interact with the binding sites. ELISA results showed that the flavonoids could effectively block PD-1/PD-L1 interactions, although the inhibitory activity of Api was weaker. Therefore, flavonols might be more effective inhibitors compared to flavones. The findings of this study are expected to contribute to the development of novel flavonoids targeting the PD-1/PD-L1 pathway.

Received 26th May 2024
Accepted 5th August 2024

DOI: 10.1039/d4ra03877k

rsc.li/rsc-advances

Introduction

Programmed cell death-1 (PD-1) and programmed cell death-ligand 1 (PD-L1) are pivotal negative immunoregulatory molecules in the tumor microenvironment.[1,2] A series of cancer cells can exploit the PD-1/PD-L1 pathway to weaken the immune capacity of T cells and escape immune surveillance. Therefore, blocking this pathway can reverse immunosuppressive states and enhance the killing of cancer cells.[3,4] Clinical success has been observed for several monoclonal antibodies targeting PD-1 (cemiplimab, nivolumab, and pembrolizumab) and PD-L1 (atezolizumab, durvalumab, and avelumab).[5,6] However, antibodies are associated with several drawbacks, such as low oral bioavailability, limited tumor permeability, immune-related adverse reactions, and high cost.[7,8] Therefore, it is urgent to explore other useful compounds for PD-1/PD-L1 blockade, including small molecules and natural products.[9,10] Several synthetic small molecules from Bristol Myers Squibb (*e.g.*, BMS1166 and BMS202) have been reported to exhibit promising inhibitory activities to interrupt PD-1/PD-L1 interactions. Co-crystallography studies have disclosed a mechanism of direct binding to PD-L1, which induces the dimerization of PD-L1.[11,12] Since then, many highly efficient small molecule inhibitors that can induce the formation of the PD-L1 dimer have been successively designed.[9,13]

Recently, natural products have attracted great attention due to their lower toxicity and multiple pharmacological effects. Among them, polyphenols account for a relatively large proportion and can intervene in all stages of tumorigenesis and development by regulating multiple signaling pathways involved in different types of cancers.[14,15] Interestingly, several polyphenols such as apigenin, curcumin, and resveratrol have been proven to be competitive inhibitors that block PD-1/PD-L1 interactions by binding to the PD-L1 dimer.[16,17] However, there is a notable lack of comparative studies regarding the effect of polyphenol structures on their binding properties. Among polyphenols, flavonoids are the most prevalent, characterized by a C6–C3–C6 skeleton consisting of two phenyl rings (A and B) linked *via* an oxygen heterocycle (C).[18–21] Structurally, flavonoids can be categorized into 3-hydroxy flavonoids and 3-desoxy flavonoids based on the presence or absence of a hydroxyl group at the 3-position on the C-ring.[18–21] Flavones lack the 3-hydroxyl group, while flavonols can be considered the 3-hydroxy derivatives of flavones.[18–21] To explore the impact of structures on binding characteristics, representative flavonoids apigenin (Api), kaempferol (Kmp), and quercetin (Que) were chosen.

In this study, molecular docking of the flavonoids with the PD-L1 dimer was carried out to build the complex systems (see

[a]*College of Food Science, Shanxi Normal University, Taiyuan 030031, China. E-mail: xjg71@163.com*

[b]*Key Laboratory for Bio-based Materials and Energy of Ministry of Education, College of Materials and Energy, South China Agricultural University, Guangzhou 510630, China. E-mail: boping@scau.edu.cn*

† Electronic supplementary information (ESI) available. See DOI: https://doi.org/10.1039/d4ra03877k

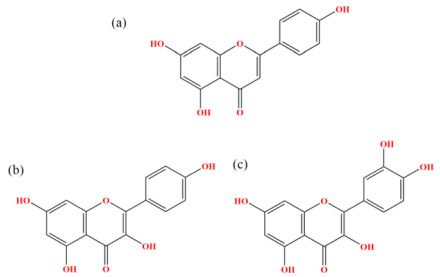

Fig. 1 Chemical structures of (a) Api, (b) Kmp and (c) Que.

Fig. 1 and 2), followed by various computational methods including molecular dynamics (MD) simulations and binding free energy calculations to determine the energy contributions of interface residues.[22,23] Subsequently, the binding modes, contact numbers, principal component analysis (PCA), and secondary structure were investigated, thereby theoretically elucidating the binding mechanism of the flavonoids on the PD-L1 dimer.[24,25] To further validate the inhibitory activities of the flavonoids on PD-1/PD-L1 interactions, ELISA (Enzyme-Linked Immunosorbent Assay) was performed. Generally, these findings may advance the development of more potent flavonoids and potentially facilitate the advancement of cancer immunotherapy.

Experimental section

Materials and methods

Molecular docking. The molecular docking studies were carried out to obtain the complex systems of the PD-L1 dimer/flavonoids.[26] The crystal structure of the PD-L1 dimer (PDB ID 5N2F) was downloaded from the PDB database. The 3D structures of the flavonoids were obtained from the PubChem database and optimized using the Gaussian 09 program[27] with the B3LYP function and def-TZVP basis sets.[28] Before docking, the PD-L1 dimer and flavonoids were converted to PDBQT format using AutoDockTools 1.5.6.[29] The docking procedure was then performed using AutoDock Vina. The grid box size and grid spacing were set to (20 Å × 20 Å × 20 Å) and 1 Å, respectively. The center of the search space was determined based on the co-crystallized ligand. The docked poses with the strongest binding affinity were considered for subsequent MD simulations. The validation of the docking approach was performed by re-docking the original crystal ligand to the PD-L1 dimer. The RMSD between the docked complex and the solved structure was 0.77 Å.[21,30] Moreover, the interaction profiles of the best-docked pose were similar to the original crystallized complex.[21,30]

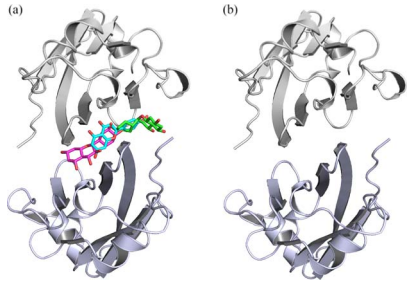

Fig. 2 The input structures for MD simulations of the (a) Api, Kmp, Que and (b) dimer systems. Api, Kmp and Que are shown in cyan, green and magenta sticks, respectively.

Molecular dynamics simulation. MD simulations of the systems obtained from molecular docking were carried out for 150 ns using the GROMACS 2016.4 package with a time step of 2 fs.[31] The AMBER ff99SB[32] and general AMBER force field (GAFF)[33] were employed to parameterize the PD-L1 dimer and flavonoids, respectively. The systems were centered in a cubic box with at least 10 Å from the edge and then dissolved in TIP3P water. Sodium and chloride ions were added to neutralize the system, followed by minimization using steepest descent and conjugate gradient methods to remove clashes. Subsequently, all systems were equilibrated at NVT and NPT ensembles for 1 ns to ensure converged systems for the further production run. The production run for the simulation was carried out at a constant temperature of 300 K and a pressure of 1 atm using the V-rescale and Parrinello–Rahman algorithms, respectively. The bond lengths involving hydrogen atoms were constrained using the LINCS algorithm. The Verlet scheme was used for the calculation of short-range non-bonded interactions with a cutoff of 1.0 nm. Particle Mesh Ewald (PME) was utilized to calculate the long-range electrostatic interactions. The trajectory and energy files were written every 10 ps for analysis.

Analysis details. The trajectories generated by MD simulations were used to analyze the root mean square deviation (RMSD), root mean square fluctuation (RMSF), contact numbers, and secondary structure of the systems using standard GROMACS tools. The interactions between the target residues and the flavonoids were calculated using the Protein–Ligand Interaction Profiler (PLIP) tool. Hydrogen bond occupancy was analyzed using Visual Molecular Dynamics (VMD) 1.9.3 software.[34] Principal component analysis (PCA) was carried out *via* the gmx covar tool to gain insights into the collective motions of the PD-L1 dimer.[35] The dynamic cross-correlation matrix (DCCM) provided information on the relevant movements of each residue on a simulation scale.

Binding free energy calculation. The binding free energy (ΔG_{bind}) between the PD-L1 dimer and flavonoids was assessed using the molecular mechanics Poisson–Boltzmann surface area (MM-PBSA) method with the g_mmpbsa tool.[36] For each system, a total of 300 snapshots were collected at intervals of 100 ps from the last equilibrated 30 ns of the MD trajectory for the calculation.

$$\Delta G = G_{complex} - (G_{protein} + G_{ligand}) \quad (1)$$

$$\Delta G_{bind} = \Delta E_{MM} + \Delta G_{sol} \quad (2)$$

$$\Delta E_{MM} = \Delta E_{ele} + \Delta E_{vdw} \quad (3)$$

$$\Delta G_{sol} = \Delta G_{PB} + \Delta G_{SA} \quad (4)$$

The $G_{complex}$, $G_{protein}$ and G_{ligand} are denoted as the free energies of the complex, PD-L1 dimer, and flavonoids, respectively (eqn (1)). ΔG_{bind} is obtained by computing the molecular mechanics energy (ΔE_{MM}) and solvation free energy (ΔG_{sol}) (eqn (2)). ΔE_{MM} is the sum of electrostatic energy (ΔE_{ele}) and van der Waals energy (ΔE_{vdW}). ΔG_{sol} consists of polar solvation energy (ΔG_{PB}) and nonpolar solvation energy (ΔG_{SA}) (eqn (3)). Among them, ΔG_{PB} and ΔG_{SA} were calculated based on the Poisson–Boltzmann (PB) equation and solvent-accessible surface area (SASA), respectively (eqn (4)). The contribution of each residue was also obtained by decomposing the binding free energy using the MM-PBSA approach.

ELISA. The PD-1/PD-L1 blockade effect of the flavonoids was determined using a PD-1 ELISA assay kit.[37] Human PD-L1 was coated onto a 96-well plate and incubated overnight at 4 °C. The plate was then washed with PBS buffer, blocked for 30 min at 37 °C, and washed again. Subsequently, the flavonoids were added and incubated for 30 min before adding human PD-1. BMS-202 was used as a positive control compound. After five washes, streptavidin–horseradish peroxidase was added, and the plate was incubated for 30 min. Then, the substrate was added and incubated for 10 min at 37 °C. After incubation, the stop solution was added, followed by measuring the absorbance optical density values at a wavelength of 450 nm.

Results and discussion

RMSD

To evaluate the structural stability of each system during the 150 ns simulation period, RMSD was calculated initially.[38] As shown in Fig. 3, the complex systems reached equilibrium after 5 ns, exhibiting relatively small fluctuations. In contrast, larger fluctuations were observed in the simulation of the PD-L1 dimer system, especially during the first 60 ns, which aligns with our previous studies.[21,30] Subsequently, these curves stabilized, indicating minimal conformational changes. The average RMSD values for the PD-L1 dimer, apigenin (Api), kaempferol (Kmp), and quercetin (Que) systems were 3.11 Å, 2.70 Å, 2.38 Å, and 2.31 Å, respectively. The higher stability observed in the complex systems may be attributed to the binding of the flavonoids. Additionally, the Api system showed larger RMSD values compared to the other two complex systems. These results illustrate that the structures of these systems maintained similarity to their initial frames throughout the simulation time, confirming stable trajectories for subsequent analysis.

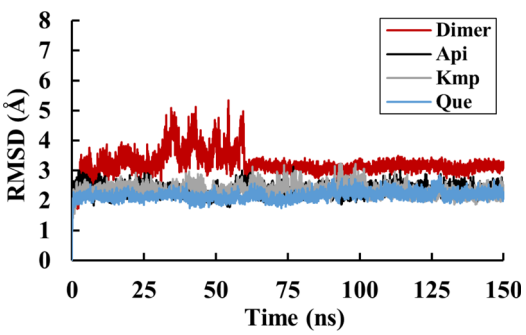

Fig. 3 RMSD values of the dimer, Api, Kmp and Que systems.

RMSF

RMSF was further examined to reveal the local fluctuations of residues in the PD-L1 dimer. As depicted in Fig. 4, all systems exhibited a similar trend in RMSF with minor variations. The N-terminal, C-terminal, and loop areas showed larger RMSF in both the PD-L1 dimer and complex systems, consistent with previous MD simulation findings.[9] Specifically, the BC loop of the PD-L1 dimer system exhibited an RMSF value of 5.1 Å. In contrast, residues in the beta sheets (A–G sheets) connected by loop domains showed comparatively less fluctuation in both unbound and bound states. Notably, the flexibility of residues in the C, F, and G sheets was notably reduced in the presence of the flavonoids. Moreover, the RMSF values of the beta sheets did not significantly differ among the complex systems. These RMSF observations are consistent with the RMSD results.

Binding free energy

To analyze the energy differences of the PD-L1 dimer upon binding to flavonoids, the MM-PBSA method was employed to calculate the binding free energy and contributions of energy components (see Table 1). As shown, the average binding free energies between the PD-L1 dimer and apigenin (Api), kaempferol (Kmp), and quercetin (Que) are -21.49 ± 0.09, -32.66 ± 0.12, and -35.39 ± 0.34 kcal mol^{-1}, respectively. This indicates that the binding abilities of Kmp and Que to the PD-L1 dimer are similar to that of curcumin but stronger than resveratrol and epigallocatechin gallate.[21] Structurally, the binding free energies between flavonols and the PD-L1 dimer appear stronger compared to flavones, possibly due to the 3-hydroxyl group on the C ring. Previous reports have suggested that the activities of flavonoids largely depend on the positions of hydroxyl groups relative to the total number of hydroxyl groups.[16] Furthermore, the binding free energy for the PD-L1 dimer system alone is 36.11 ± 0.89 kcal mol^{-1}, indicating that flavonoids play a crucial role in the formation of the PD-L1 dimer. Upon analyzing different components of the complex systems, it is evident that the binding of flavonoids to the PD-L1 dimer is predominantly mediated by van der Waals energy. The van der Waals interaction energy for the Que system is the strongest at -51.30 ± 0.31 kcal mol^{-1}, while for Api and Kmp systems, it is -40.63 ± 0.60 and -47.55 ± 0.38 kcal mol^{-1}, respectively. Electrostatic interaction energy also contributes favorably, with Que exhibiting a stronger electrostatic interaction energy (-6.44 ± 1.47 kcal mol^{-1}) compared to Api (-1.14 ± 1.39 kcal mol^{-1}) and Kmp (-4.98 ± 1.64 kcal mol^{-1}) when binding to the PD-L1 dimer, possibly due to the 3′-hydroxyl group on the B ring. In summary, polar solvation interactions can impair binding, whereas nonpolar solvation interactions are favorable for the binding process.

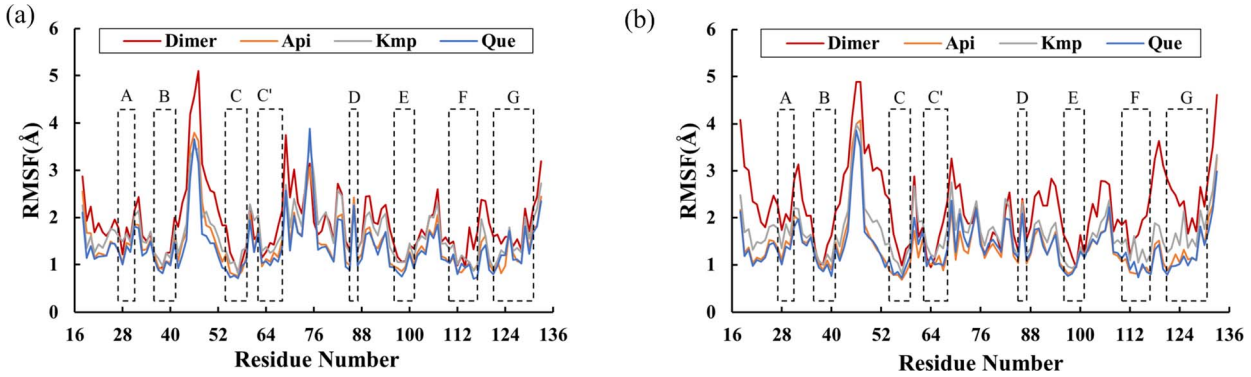

Fig. 4 RMSF values of residues on (a) $_{A}$PD-L1 and (b) $_{B}$PD-L1 of the dimer, Api, Kmp and Que systems.

Per-residue energy decomposition

For a comprehensive analysis of key residues involved in the binding of flavonoids to the PD-L1 dimer, per-residue energy decomposition was performed. As depicted in Fig. 5, In the Api system (Fig. 5a), nine residues showed binding free energy contributions exceeding −0.5 kcal mol^{-1}. Among these, $_{B}$Ile54, $_{B}$Tyr56, and $_{B}$Met115 were major contributors, with $_{B}$Tyr56 exerting the most significant negative impact at −2.20 kcal mol^{-1}. In the Kmp system (Fig. 5b), 16 residues interacted strongly with the PD-L1 dimer, each contributing more than −0.5 kcal mol^{-1}. Notably, $_{A}$Met115, $_{A}$Ala121, $_{B}$Ile54, $_{B}$Tyr56, $_{B}$Met115, $_{B}$Ile116, $_{B}$Ser117, and $_{B}$Ala121 contributed over −1 kcal mol^{-1}. The total interaction energies of these residues with Kmp ranged from −1.00 to −2.60 kcal mol^{-1}. Compared to the Api system, $_{A}$Tyr123, $_{B}$Ile54, and $_{B}$Tyr56 in the Kmp system showed slightly attenuated contributions (by 0.21 to 0.86 kcal mol^{-1}), while contributions of other residues, particularly $_{A}$Ile54 and $_{A}$Tyr56, were enhanced. In the Que system (Fig. 5c), 15 residues had binding free energy contributions exceeding −0.5 kcal mol^{-1}. Key residues like $_{A}$Ile54, $_{A}$Tyr56, $_{A}$Met115, $_{A}$Ile116, $_{A}$Ser117, $_{A}$Ala121, $_{A}$Asp122, $_{B}$Met115, $_{B}$Ala121, and $_{B}$Y56 contributed over −1 kcal mol^{-1}. Notably, $_{A}$Met115 showed an enhanced interaction with Que by 0.76 kcal mol^{-1} compared to Kmp. The role of Met115 in small-molecule binding has been underscored in previous studies.[9,39,40] Comparative analysis indicated that residues Ile54, Tyr56, Met115, Ala121, and Tyr123 play crucial roles in binding to flavonoids, with varying contributions across different systems. These residues are known to be involved in constructing active binding sites between PD-1 and PD-L1, as reported in experimental and computational studies.[9,39,40] Additionally, compared to the Que system, the Api and Kmp systems showed a more concentrated distribution of key residues in the binding domain of $_{B}$PD-L1. In summary, these results suggest that flavonoids effectively bind to the PD-L1 dimer, thereby potentially inhibiting PD-1/PD-L1 interactions.

Contact numbers

To determine the binding sites of flavonoids on the PD-L1 dimer, the average number of contacts between each residue and flavonoids was calculated.[41] As depicted in Fig. 6, Api (Fig. 6a) predominantly binds to the residues $_{A}$Met115, $_{A}$Ala121, $_{A}$Asp122, $_{A}$Tyr123, $_{B}$Ile54, $_{B}$Val55, $_{B}$Tyr56, $_{B}$Gln66, $_{B}$Ile116, $_{B}$Ser117, and $_{B}$Ala121, each with an average contact number greater than 10, though the specific values vary slightly. Notably, $_{B}$Tyr56 shows the highest contact number (27 contacts) among all residues, particularly in the C sheet, with Api. Kmp (Fig. 6b) and Que (Fig. 6c) exhibit relatively high contact numbers with the residues including Ile54, Tyr56, Met115, Ile116, Ser117, Ala121, Asp122, and Tyr123 in both $_{A}$PD-L1 and $_{B}$PD-L1. $_{A}$Ala121 and $_{B}$Ala121 have the highest contact numbers with Kmp and Que, respectively. Additionally, Que preferentially contacts $_{A}$Gln66 and $_{A}$Val55. Kmp and Que also show significant interactions with $_{A}$Ile54, $_{A}$Tyr56, $_{B}$Ala121, $_{B}$Asp122, and $_{B}$Tyr123,

Table 1 Binding free energies of the dimer, Api, Kmp and Que systems (kcal mol^{-1})

Contribution	Api	Kmp	Que	Dimer
ΔE_{vdw}[a]	−40.63 ± 0.60	−47.55 ± 0.38	−51.30 ± 0.31	−44.59 ± 9.85
ΔE_{ele}[b]	−1.14 ± 1.39	−4.98 ± 1.64	−6.44 ± 1.47	−124.35 ± 23.36
ΔE_{PB}[c]	23.51 ± 2.05	23.54 ± 1.33	25.99 ± 1.58	211.28 ± 17.07
ΔE_{SA}[d]	−3.24 ± 0.08	−3.66 ± 0.07	−3.64 ± 0.06	−6.23 ± 0.37
$\Delta E_{polar,total}$[e]	22.37 ± 0.75	18.56 ± 0.32	19.55 ± 0.52	86.94 ± 10.00
$\Delta E_{nonpolar,total}$[f]	−43.86 ± 0.68	−51.21 ± 0.44	−54.94 ± 0.36	−50.82 ± 10.06
ΔG[g]	−21.49 ± 0.09	−32.66 ± 0.12	−35.39 ± 0.34	36.11 ± 0.89

[a] van der Waals interaction energy. [b] Electrostatic energy. [c] Polar solvent effect energy. [d] Nonpolar solvent effect energy. [e] Polar binding free energy. [f] Nonpolar binding free energy. [g] Binding free energy.

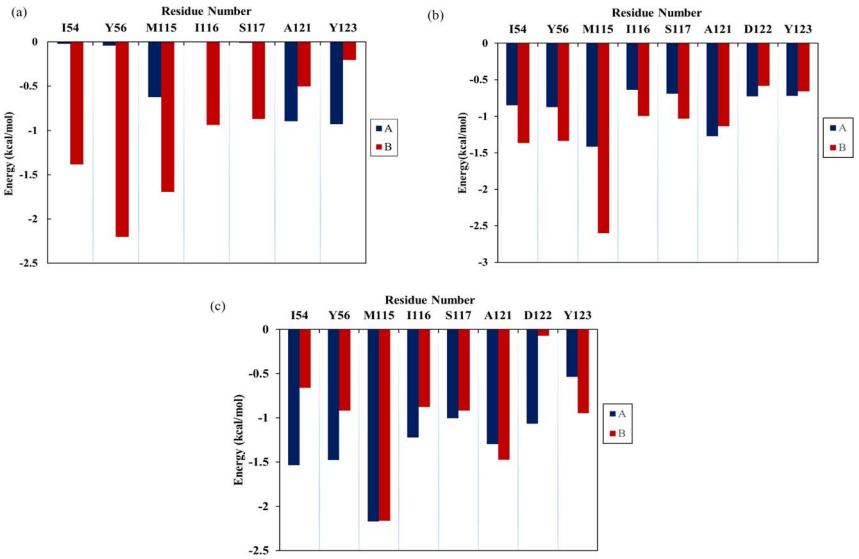

Fig. 5 The contribution of residues of the PD-L1 dimer in complex with three flavonoids, (a) Api, (b) Kmp and (c) Que.

especially $_{A}$Ile54 and $_{A}$Tyr56, compared to Api. Overall, Kmp and Que exhibit notably higher contact numbers (ranging from 310 to 329) with the PD-L1 dimer compared to Api, primarily due to interactions in the β-sheet regions. These findings are consistent with the calculated binding free energies presented in Table 1 and Fig. 5. Interestingly, residues with high contact numbers are located in the C sheet (residues 54–56), C′ sheet (residues 66–68), F sheet (residues 115–117), and G sheet (residues 121–124), which are crucial for forming and stabilizing the PD-1/PD-L1 binding interface. This suggests that flavonoids can bind closely to the PD-L1 dimer, thereby potentially blocking PD-1/PD-L1 interactions.

Non-bonded interactions

In the protein–ligand systems, intermolecular hydrogen bonds contribute significantly to stabilizing ligands within binding pockets.[26] The hydrogen bond occupancies between the PD-L1 dimer and flavonoids throughout the equilibration period were calculated and summarized in Table 2. For Api, the NZ atom of $_{A}$Lys124 forms one hydrogen bond with an occupancy of 16.28%. This interaction is crucial as $_{A}$Lys124 acts as a hydrogen donor. In the Kmp system, the O atom of the negatively charged $_{A}$Asp122 forms two hydrogen bonds, one with the O27 atom (51.16% occupancy) and another with the O29 atom (50.16% occupancy) of Kmp, serving as hydrogen acceptors. These bonds are pivotal for maintaining the binding stability of this system

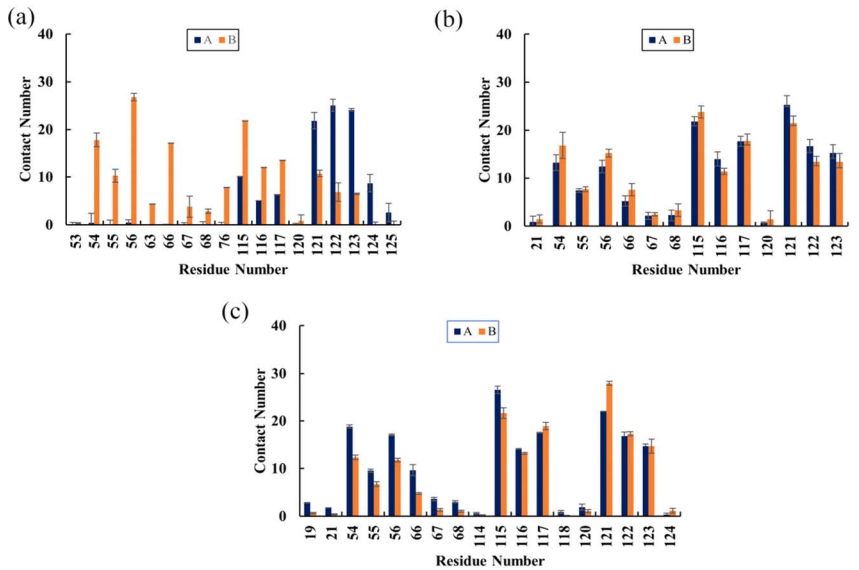

Fig. 6 The average contact numbers between the PD-L1 dimer and (a) Api, (b) Kmp and (c) Que. The error bars represent the standard of the mean.

Table 2 Hydrogen bond occupancies of the Api, Kmp and Que systems

Donor	Donor H	Acceptor	Occupancy (%)
$_{A}$Lys124@NZ	HZ1	Api@OAB	16.28
Kmp@O27	HO27	$_{A}$Asp122@O	51.16
Kmp@O29	HO29	$_{A}$Asp122@O	50.17
Que@O29	HO29	$_{A}$Gln66@OE1	85.05
Que@O27	HO27	$_{A}$Ile116@O	59.14

due to their occupancies exceeding 50%.[42] In the Que system, the highest hydrogen bond occupancy (85.05%) occurs between the OE1 atom of $_{A}$Gln66 and the O29 atom of Que. Additionally, the O atom of $_{A}$Ile116 forms a stable hydrogen bond with the O27 atom of Que with an occupancy of 59.14%. This strong interaction may be attributed to more hydroxyl groups in the B ring of Que compared to Api and Kmp. These results align with the weaker electrostatic contribution to the binding energy observed in the Api system (ΔE_{ele} in Table 1) compared to the other complex systems. Importantly, these residues have been identified in previous studies as critical for binding to the PD-L1 dimer.[9,39,40] Therefore, these stable hydrogen bonds likely contribute significantly to the inhibitory activity of flavonoids against the PD-1/PD-L1 pathway.

The binding modes of the representative complex structures were analyzed, as depicted in Fig. 7, revealing predominantly hydrophobic interactions. Here are the specific interactions observed, residues $_{A}$Tyr123, $_{B}$Tyr56, and $_{B}$Met115 are involved in binding with Api. Additionally, a hydrogen bond is formed between Api and $_{A}$Lys124. Residues $_{A}$Ile54, $_{A}$Met115, $_{A}$Ala121, $_{B}$Ile54, $_{B}$Tyr56, $_{B}$Met115, $_{B}$Ala121, and $_{B}$Tyr123 are directly involved in binding with Kmp. Six hydrogen bonds are observed between Kmp and $_{A}$Ile116, $_{A}$Ala121, $_{A}$Asp122, $_{B}$Ile54, and $_{B}$Met115. Residues $_{A}$Tyr56, $_{A}$Met115, $_{A}$Ala121, $_{A}$Tyr123, and $_{B}$Ala121 are directly involved in binding with Que. Six hydrogen bonds are formed between Que and $_{A}$Ile54, $_{A}$Gln66, $_{A}$Ile116, $_{A}$Asp122, and $_{B}$Tyr123. In summary, while all studied flavonoids bind to the PD-L1 dimer, the specific residues involved in these interactions differ. Notably, these interactions predominantly involve small polar interactions and relatively large hydrophobic interactions. Moreover, the Kmp and Que systems exhibit stronger hydrogen bond interactions compared to the Api system, which can be attributed to their higher number of hydroxyl groups. These findings underscore the diverse binding mechanisms and the potential differences in binding affinity among flavonoids, highlighting their distinct modes of interaction with the PD-L1 dimer.

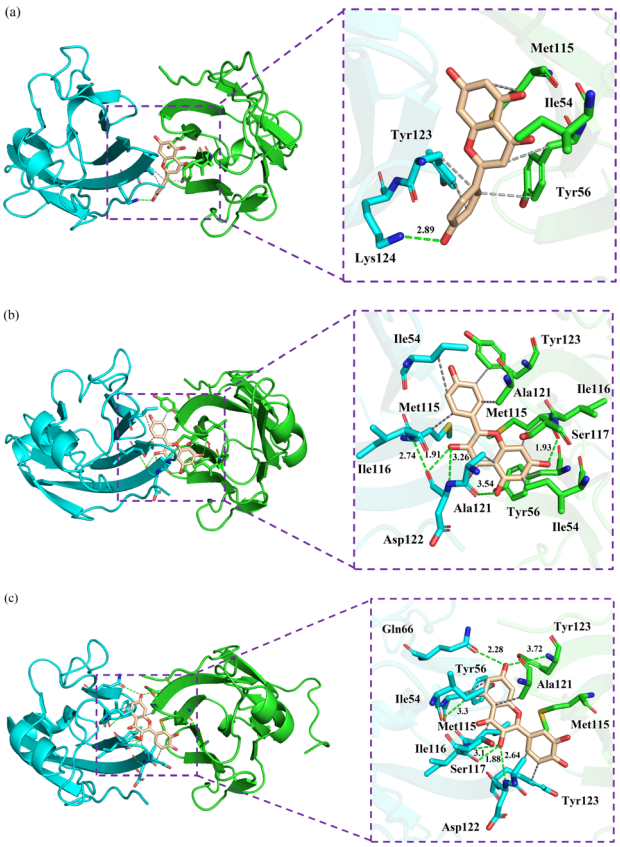

Fig. 7 The binding modes of the PD-L1 dimer in complex with (a) Api, (b) Kmp and (c) Que. The residues are shown as sticks with $_{A}$PD-L1 and $_{B}$PD-L1 coloured cyan and green, respectively. The hydrophobic interactions and hydrogen bonds are shown as grey and green dashes, respectively.

Dynamic cross-correlation matrix analysis

Dynamic cross-correlation matrix (DCCM) analysis was conducted to examine the dynamical motions among Cα atoms of the PD-L1 dimer.[43] In the DCCM, positive areas (red) indicate correlated motions among residues, while negative areas (blue) indicate anti-correlated movements. The intensity of colors reflects the degree of correlation. As illustrated in Fig. 8, the N-terminal and C-terminal regions, such as residues $_{A}$Ala0 to $_{A}$Asp8 (corresponding to residues $_{A}$Ala18 to $_{A}$Asp26), show a red block within each system, suggesting correlated motions. These

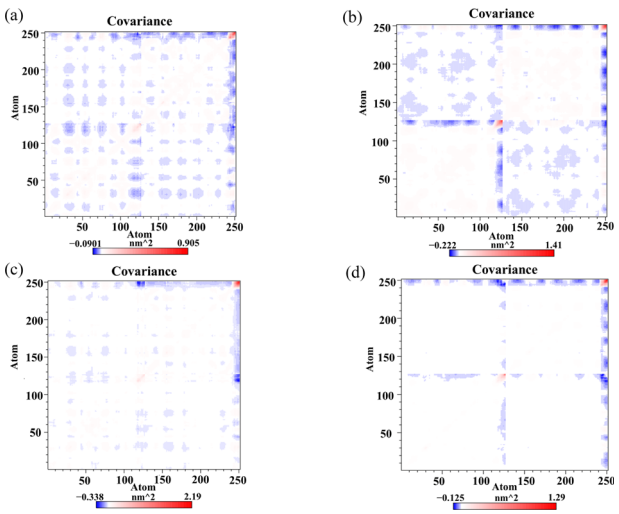

Fig. 8 Dynamic cross-correlation matrix of the (a) dimer, (b) Api, (c) Kmp and (d) Que systems.

areas are typically distant from the binding sites and may exhibit similar dynamics across different systems. The unbound PD-L1 dimer shows the highest anti-correlated movements, depicted by extensive blue regions. This indicates diverse and independent motions of residues in the absence of ligand. The Api-bound PD-L1 dimer displays higher correlated motions compared to the unbound dimer, particularly evident in most areas of the protein. This suggests that Api binding induces more coordinated motions among residues, possibly due to specific interactions stabilizing the complex. Both Kmp and Que bound to the PD-L1 dimer exhibit maximum correlated motions compared to Api. This enhanced correlation can be attributed to their tighter interactions with the PD-L1 dimer, resulting in more concerted movements among residues. In summary, the DCCM analysis provides insights into how flavonoid binding affects the dynamical motions of the PD-L1 dimer. It underscores the differential impact of Api, Kmp, and Que on the correlated motions within the PD-L1 dimer, reflecting their varying degrees of binding affinity and stabilization mechanisms.

Secondary structure

The DSSP program was used to gain insight into the effect of the flavonoids on the secondary structures of the PD-L1 dimer. According to Fig. 9, no apparent changes were observed in the secondary structure of the PD-L1 dimer when binding with the flavonoids compared to the dimer system. The beta-sheet conformation of the PD-L1 dimer remained almost entirely stable throughout the 150 ns MD simulations. Importantly, the C, F, and G sheet domains are crucial for the recognition of the flavonoids, as mentioned earlier. Additionally, as the simulation progressed, the secondary structure of other domains mainly transformed between coil, α-helix, bend, and turn. In general, secondary structure analysis clearly indicated the formation of stable and compact complexes.

PD-1/PDL-1 inhibitory activity

The blockade effects of the flavonoids on PD-1/PD-L1 interactions were tested using an ELISA assay. The PD-1/PD-L1 small-molecule inhibitor BMS-202, which recognizes the extracellular domain of PD-L1 and blocks PD-1/PD-L1 interactions, was used as a positive control.[44] The results showed that BMS-202 dose-dependently inhibited the interaction between PD-1 and PD-L1 with an IC_{50} value of 9.94 μg mL^{-1}. To determine whether the flavonoids possess inhibitory effects on PD-1/PD-L1 interactions, a comparative study was performed. As illustrated in Fig. 10, Api showed a smaller blockade effect with an IC_{50} of 134.85 μg mL^{-1}. Moreover, Kmp and Que also revealed

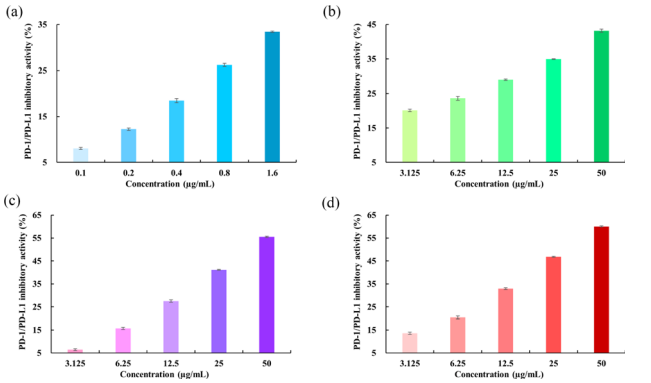

Fig. 10 Inhibitory activities of (a) BMS-202, (b) Api, (c) Kmp and (d) Que on PD-1/PD-L1 interactions.

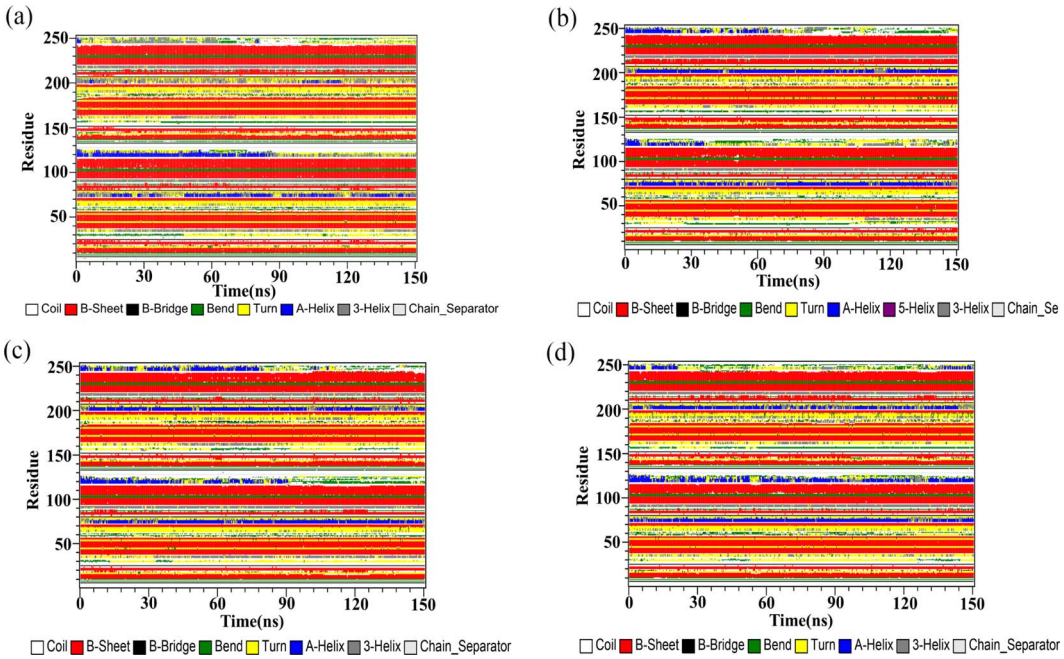

Fig. 9 The secondary structures of the PD-L1 dimer in the (a) dimer, (b) Api, (c) Kmp and (d) Que systems.

inhibitory impacts on PD-1/PD-L1 binding, with activities of 39.72 and 29.93 μg mL^{-1}, respectively, following a similar trend to the binding free energy of the complex systems as mentioned above. These findings indicated that Api, Kmp, and Que are effective PD-1/PD-L1 blockaders, and further studies can focus on flavonoids with similar structural skeletons.

Conclusions

In this paper, molecular modeling and experimental approaches were employed to explore the interaction mechanism between the PD-L1 dimer and the flavonoids Api, Kmp, and Que. The binding free energy calculations revealed that the binding of flavonoids to the PD-L1 dimer was spontaneous, with Kmp and Que showing stronger binding abilities than Api. Notably, the residues Ile54, Tyr56, Met115, Ala121, and Tyr123 contributed significantly to the binding. Furthermore, the structural basis, specifically the C-, F-, and G-sheet regions, for the binding of the flavonoids with the PD-L1 dimer was elucidated *via* contact number analysis. The interaction analysis showed that the active cavity is mainly driven by hydrophobic interactions. The analysis of DCCM and secondary structure further indicated that the flavonoids could stably interact with the binding regions. Consistent with the dynamics data, the ELISA results demonstrated that the flavonoids inhibited PD-1/PD-L1 interactions in a concentration-dependent manner, with Kmp and Que showing stronger activities than Api. In summary, this study offers useful information for the further development of flavonoids targeting the PD-1/PD-L1 pathway.

Data availability

Autodock Vina and MGLTools were used for molecular docking, which can be obtained free of charge: **https://vina.scripps.edu/downloads/** and **https://ccsb.scripps.edu/mgltools/downloads/**. GROMACS 2016.4 was used for MD simulations at 300 K, which can be obtained free of charge: **https://manual.gromacs.org/2016.4/download.html**. AmberTools23 was used to parameterize the force field of the flavonoids, which can be obtained from **https://ambermd.org/GetAmber.php#ambertools**. VMD 1.9.3 was used to compute the occupancies of intermolecular H bonds, which can be obtained free of charge: **https://www.ks.uiuc.edu/Research/vmd/vmd-1.9.3/**. PyMOL 2.5 was used for visualization, which can be obtained free of charge: **https://pymol.org/2/**. The WHAT IF online server was used to complete the PD-L1 dimer, which can be obtained free of charge: **https://swift.cmbi.umcn.nl/servers/html/index.html**. PLIP was used to compute non-bonded interactions, which can be obtained free of charge: **https://plip-tool.biotec.tu-dresden.de/plip-web/plip/index**.

Author contributions

Yan Guo: writing – original draft, methodology, investigation, formal analysis, and conceptualization. Jinchang Tong: investigation, and investigation. Kaixin Shi, Xinyue Song, and Zichao Guo: investigation, and date analysis. Jianhuai Liang: conceptualization, formal analysis, and writing – review and editing. Boping Liu and Jianguo Xu: conceptualization, and writing – review & editing.

Conflicts of interest

There are no conflicts to declare.

Acknowledgements

This research was funded by the Natural Science Foundation (202203021212392) of Shanxi Province and Technological Innovation Program in Higher Education Institutions (No. 2022L262) of Shanxi Province.

Notes and references

1 J. J. Park, E. P. Thi, V. H. Carpio, *et al.*, Checkpoint inhibition through small molecule-induced internalization of programmed death-ligand 1, *Nat. Commun.*, 2021, **12**, 1222.
2 V. Kumar, A. Bahuguna and M. Kim, Molecular insights into binding of bioactive compounds from essential oil of Trachyspermum ammi with human programmed cell death protein 1, *J. Biomol. Struct. Dyn.*, 2023, 1–11.
3 Q. Wu, L. Jiang, S. Li, *et al.*, Small molecule inhibitors targeting the PD-1/PD-L1 signaling pathway, *Acta Pharmacol. Sin.*, 2021, **42**, 1–9.
4 G. R. Sartori, A. O. Albuquerque, A. H. Santos-Costa, *et al.*, In silico mapping of the dynamic interactions and structure-activity relationship of flavonoid compounds against the immune checkpoint programmed-cell death 1 pathway, *Front. Drug Discov.*, 2022, **2**, 1032587.
5 C. Liu, N. P. Seeram and H. Ma, Small molecule inhibitors against PD-1/PD-L1 immune checkpoints and current methodologies for their development: a review, *Cancer Cell Int.*, 2021, **21**, 239.
6 H. Li, N. P. Seeram, C. Liu, *et al.*, Further investigation of blockade effects and binding affinities of selected natural compounds to immune checkpoint PD-1/PD-L1, *Front. Oncol.*, 2022, **12**, 995461.
7 E. Domingo-Contreras, J. R. Tormo, V. Gonzalez-Menendez, *et al.*, Discovery of bioactive natural products of microbial origin as inhibitors of the PD-1/PD-L1 protein-protein interaction, *Int. J. Biol. Macromol.*, 2024, **264**, 130458.
8 H. Zheng, G. Wang, M. Liu, *et al.*, Traditional Chinese medicine inhibits PD-1/PD-L1 axis to sensitize cancer immunotherapy: a literature review, *Front. Oncol.*, 2023, **13**, 1168226.
9 X. Xu, S. Luo, X. Zhao, *et al.*, Computational analysis of PD-L1 dimerization mechanism induced by small molecules and potential dynamical properties, *Int. J. Biol. Macromol.*, 2024, **265**, 130921.
10 N. S. Alharthi, M. S. Alwethaynani, A. Y. Alhazmi, *et al.*, In silico assessment of a natural small molecule as an inhibitor of programmed death ligand 1 for cancer

immunotherapy: a computational approach, *J. Biomol. Struct. Dyn.*, 2024, 1–21.
11 K. M. Zak, P. Grudnik, K. Guzik, *et al.*, Structural basis for small molecule targeting of the programmed death ligand 1 (PD-L1), *Oncotarget*, 2016, **7**, 30323.
12 L. Skalniak, K. M. Zak, K. Guzik, *et al.*, Small-molecule inhibitors of PD-1/PD-L1 immune checkpoint alleviate the PD-L1-induced exhaustion of T-cells, *Oncotarget*, 2017, **8**, 72167.
13 Y. OuYang, J. Gao, L. Zhao, *et al.*, Design, synthesis, and evaluation of o-(biphenyl-3-ylmethoxy) nitrophenyl derivatives as PD-1/PD-L1 inhibitors with potent anticancer efficacy in vivo, *J. Med. Chem.*, 2021, **64**, 7646–7666.
14 D. Tewari, P. Patni, A. Bishayee, *et al.*, Natural products targeting the PI3K-Akt-mTOR signaling pathway in cancer: a novel therapeutic strategy, *Semin. Cancer Biol.*, 2022, **80**, 1–17.
15 M. Moloudizargari, M. H. Asghari, S. F. Nabavi, *et al.*, Targeting Hippo signaling pathway by phytochemicals in cancer therapy, *Semin. Cancer Biol.*, 2022, **80**, 183–194.
16 J. G. Choi, Y. S. Kim, J. H. Kim, *et al.*, Anticancer effect of *Salvia plebeia* and its active compound by improving T-cell activity via blockade of PD-1/PD-L1 interaction in humanized PD-1 mouse model, *Front. Immunol.*, 2020, **11**, 598556.
17 Y. Guo, J. Liang, B. Liu, *et al.*, Molecular mechanism of food-derived polyphenols on PD-L1 dimerization: a molecular dynamics simulation study, *Int. J. Mol. Sci.*, 2021, **22**, 10924.
18 C. Papuc, G. V. Goran, C. N. Predescu, *et al.*, Plant polyphenols as antioxidant and antibacterial agents for shelf-life extension of meat and meat products: classification, structures, sources, and action mechanisms, *Compr. Rev. Food Sci. Food Saf.*, 2017, **16**, 1243–1268.
19 A. Silva, V. Silva, G. Igrejas, *et al.*, Phenolic compounds classification and their distribution in winemaking by-products, *Eur. Food Res. Technol.*, 2023, **249**, 207–239.
20 L. Li, X. Yan, F. Chen, *et al.*, A comprehensive review of the metabolism of citrus flavonoids and their binding to bitter taste receptors, *Compr. Rev. Food Sci. Food Saf.*, 2023, **22**, 1763–1793.
21 D. Shah, M. Gandhi, A. Kumar, *et al.*, Current insights into epigenetics, noncoding RNA interactome and clinical pharmacokinetics of dietary polyphenols in cancer chemoprevention, *Crit. Rev. Food Sci.*, 2023, **63**, 1755–1791.
22 A. Belhassan, S. Chtita, H. Zaki, *et al.*, In silico detection of potential inhibitors from vitamins and their derivatives compounds against SARS-CoV-2 main protease by using molecular docking, molecular dynamic simulation and ADMET profiling, *J. Mol. Struct.*, 2022, **1258**, 132652.
23 Y. Liao, Y. Ding, L. Yu, *et al.*, Exploring the mechanism of Alisma orientale for the treatment of pregnancy induced hypertension and potential hepato-nephrotoxicity by using network pharmacology, network toxicology, molecular docking and molecular dynamics simulation, *Front. Pharmacol*, 2022, **13**, 1027112.
24 Z. Yang, X. Fu, Y. Zhao, *et al.*, Molecular insights into the inhibition mechanism of harringtonine against essential proteins associated with SARS-CoV-2 entry, *Int. J. Biol. Macromol.*, 2023, **240**, 124352.
25 Z. A. Bhat, M. M. Khan, A. Rehman, *et al.*, MD simulations indicate Omicron P132H of SARS-CoV-2 Mpro is a potential allosteric mutant involved in modulating the dynamics of catalytic site entry loop, *Int. J. Biol. Macromol.*, 2024, 130077.
26 P. Dashtestani and L. Karami, The molecular mechanism of the effects of the anti-neuropathic ligands on the modulation of the sigma-2 receptor: an in-silico study, *Int. J. Biol. Macromol.*, 2024, **254**, 127925.
27 M. J. Frisch, G. W. Trucks, H. B. Schlegel, *et al.*, *Gaussian 09*, Gaussian, Inc., Wallingford CT, 2016.
28 S. Grimme, S. Ehrlich and L. Goerigk, Effect of the damping function in dispersion corrected density functional theory, *J. Comput. Chem.*, 2011, **32**, 1456–1465.
29 F. Liang, K. Meng, X. Pu, *et al.*, Deciphering the binding behavior and interaction mechanism of apigenin and α-glucosidase based on multi-spectroscopic and molecular simulation studies, *Int. J. Biol. Macromol.*, 2024, 130535.
30 Y. Guo, Y. Jin, B. Wang, *et al.*, Molecular mechanism of small-molecule inhibitors in blocking the PD-1/PD-L1 pathway through PD-L1 dimerization, *Int. J. Mol. Sci.*, 2021, **22**, 4766.
31 S. L. Jiang, Z. Y. Hu, W. J. Wang, *et al.*, Investigation on the binding behavior of human α1-acid glycoprotein with Janus kinase inhibitor baricitinib: multi-spectroscopic and molecular simulation methodologies, *Int. J. Biol. Macromol.*, 2023, 125096.
32 M. J. Abraham, T. Murtola, R. Schulz, *et al.*, GROMACS: high performance molecular simulations through multi-level parallelism from laptops to supercomputers, *SoftwareX*, 2015, **1**, 19–25.
33 J. Wang, R. M. Wolf, J. W. Caldwell, *et al.*, Development and testing of a general amber force field, *J. Comput. Chem.*, 2004, **25**, 1157–1174.
34 J. Liu, B. Li, Z. Li, *et al.*, Deciphering the alkaline stable mechanism of bacterial laccase from Bacillus pumilus by molecular dynamics simulation can improve the decolorization of textile dyes, *J. Hazard. Mater.*, 2023, **443**, 130370.
35 Y. Pan, C. Zhao, W. Fu, *et al.*, Comparative analysis of structural dynamics and allosteric mechanisms of RecA/Rad51 family proteins: integrated atomistic MD simulation and network-based analysis, *Int. J. Biol. Macromol.*, 2024, **261**, 129843.
36 B. Pandey and A. Grover, Mechanistic and structural insight into R2R3-MYB transcription factor in plants: molecular dynamics based binding free energy analysis, *J. Biomol. Struct. Dyn.*, 2024, **42**, 2632–2642.
37 H. F. Li, N. P. Seeram, C. Liu, *et al.*, Further investigation of blockade effects and binding affinities of selected natural compounds to immune checkpoint PD-1/PD-L1, *Front. Oncol.*, 2022, **12**, 995461.
38 J. F. Cao, X. Yang, L. Xiong, *et al.*, Exploring the mechanism of action of dapansutrile in the treatment of gouty arthritis

based on molecular docking and molecular dynamics, *Front. Physiol.*, 2022, **13**, 990469.

39 C. Sun, Y. Cheng, X. Liu, *et al.*, Novel phthalimides regulating PD-1/PD-L1 interaction as potential immunotherapy agents, *Acta Pharm. Sin. B*, 2022, **12**, 4446–4457.

40 R. Butera, M. Ważyńska, K. Magiera-Mularz, *et al.*, Design, synthesis, and biological evaluation of imidazopyridines as PD-1/PD-L1 antagonists, *ACS Med. Chem. Lett.*, 2021, **12**, 768–773.

41 X. Li, Y. Zhang, Z. Yang, *et al.*, The Inhibition Effect of Epigallocatechin-3-Gallate on the Co-Aggregation of Amyloid-β and Human Islet Amyloid Polypeptide Revealed by Replica Exchange Molecular Dynamics Simulations, *Int. J. Mol. Sci.*, 2024, **25**, 1636.

42 S. H. Mirmajidi, C. Irajie, A. Savardashtaki, *et al.*, Identification of potential RapJ hits as sporulation pathway inducer candidates in Bacillus coagulans via structure-based virtual screening and molecular dynamics simulation studies, *J. Mol. Model.*, 2023, **29**, 256.

43 D. Zhan, S. Guan, H. Jin, *et al.*, Stereoselectivity of phosphotriesterase with paraoxon derivatives: a computational study, *J. Biomol. Struct. Dyn.*, 2016, **34**, 600–611.

44 K. Guzik, K. M. Zak, P. Grudnik, *et al.*, Small-Molecule inhibitors of the programmed cell death-1/programmed death-ligand 1 (PD-1/PD-L1) interaction via transiently induced protein states and dimerization of PD-L1, *J. Med. Chem.*, 2017, **60**, 5857–5867.